


Bearing Capacity of Embedded Strip Footings on Cohesionless Soil Under Vertical and Horizontal Loads

Hadjer Yahia-Cherif  · Abdelhak Mabrouki · Djamel Benmeddour · Mekki Mellas

Received: 18 February 2016 / Accepted: 3 November 2016 / Published online: 10 November 2016
© Springer International Publishing Switzerland 2016

Abstract In the last decades a few attention was given to the evaluation of the bearing capacity of embedded footing under inclined loads on a frictional soil. This paper focuses on a numerical study using the finite-difference code Fast Lagrangian Analysis of Continua (FLAC), to evaluate the bearing capacity of embedded strip footing on a frictional soil. The soil is modeled by an elasto-plastic model with a Mohr–Coulomb yield criterion and associative flow rule; the effect of non-associativity of the soil on the bearing capacity is also investigated. The effect of the embedment is estimated through a depth factor, defined as a ratio of the bearing capacity of a strip footing at a depth D to that of a strip footing at the ground surface. The inclination effect is estimated by inclination factors, defined as the ratio of the limit vertical load for a footing under inclined loading to that of the vertically loaded footing. Both swipe and probe analyses were carried out to identify the vertical force–horizontal force (V–H) failure envelope. The results have been compared with those available in the literature.

Keywords Bearing capacity · Depth factors · Vertical loads · Inclined loads · Numerical modelling · Strip footing · Cohesionless soil

1 Introduction

Bearing capacity calculations are an important part of the design of foundations. The bearing capacity of a vertically loaded strip footing is generally evaluated using the superposition formula proposed by Terzaghi (1943). Terzaghi's equation is based on the superposition principle to combine the effects of cohesion, surcharge, and soil weight. The resulting bearing capacity is expressed as:

$$q_u = \frac{1}{2} \gamma B N_\gamma + c N_c + q N_q \quad (1)$$

where γ is the unit weight, c the cohesion, B the width of the strip footing; N_c , N_q and N_γ are the bearing capacity factors, which represent the effects of the soil cohesion c , the surcharge q , and the soil unit weight γ , respectively. These bearing capacity factors depend only on the internal friction angle ϕ of the soil under the footing.

Many analytical and numerical methods can be used to calculate the vertical bearing capacity of a rigid strip footing; the limit equilibrium method is the most popular in practice because of its relative simplicity. In this method, collapse is assumed to

H. Yahia-Cherif (✉) · A. Mabrouki ·
D. Benmeddour · M. Mellas
Department of Civil and Hydraulic Engineering,
University of Biskra, BP 145, 07000 Biskra, Algeria
e-mail: hadjer_yahia@yahoo.fr

occur as a result of sliding on a rupture surface and the failure criterion is assumed to be satisfied within the soil mass (Terzaghi 1943; Meyerhof 1951; Vesic 1973; Kumbhojkar 1993).

By means of the method of characteristics, commonly referred to as the slip-line method, Lundgren and Mortensen (1953), Hansen (1961), Bolton and Lau (1993) and Martin (2003) studied the bearing capacity of shallow foundations. This method based on integrating the equations of plastic equilibrium and is more rigorous.

Moreover, many researchers have used the limit analysis method to study the bearing capacity (Chen 1975; Michalowski 1997; Soubra 1999; Hjiatj et al. 2005). Limit analysis method includes upper bound and lower bound theorems. Limit analysis method includes upper bound and lower bound theorems. Michalowski (2005) indicated that the limit analysis theorems requires normality of the flow (associativity), therefore the theorems are not valid for soils that are governed by the nonassociative flow rule. The displacement finite element or finite-difference technique can also be used to derive approximate estimates of the bearing capacity (Frydman and Burd 1997; Yin et al. 2001; Erickson and Drescher 2002; Mabrouki et al. 2010; Loukidis and Salgado 2009). In this method, the shape and the failure mechanism are not necessary.

Current studies of bearing capacity for shallow foundations tend to rely on the hypothesis of a surface footing subjected to vertical loads. In practice, the footing is embedded in soil and subjected to inclined loads due to vertical V and horizontal H loads transmitted by the superstructure or inclined columns such as is transmission towers. To take into account, the effects of embedment and inclined loading, the conventional bearing capacity Eq. (1) is modified by the correction factors. The bearing capacity formula can be written as:

$$q_u = \frac{1}{2} \gamma B N_\gamma d_\gamma i_\gamma + c N_c d_c i_c + q N_q d_q i_q \quad (2)$$

where d_γ , d_c and d_q are the depth factors, i_γ , i_c and i_q are the inclination factors.

Many researchers have investigated the problem of a surface strip footing on sand subjected to inclined loads. Meyerhof (1953) used the method of limit equilibrium to calculate the bearing capacity of foundations under inclined loads, for two different

failure mechanisms, one for small inclinations and another for large inclinations. Also, Meyerhof (1963) proposed a depth factor for estimate the increase of bearing capacity by the shearing resistance of the soil above the foundation level. Furthermore, Hansen (1970) proposed a formula for depth and load inclination factors. Vesic (1975) proposed empirical modifications to Hansen's expressions for the inclination factors. Tani and Craig (1995) suggested that the bearing capacity of a shallow foundation is independent of the soil strength above the level of the base of the footing (there were no embedment effects). Recently, Lyamin et al. (2007) presented results of rigorous analyses that employ to obtain values of depth factors for use in bearing capacity computations in the sand using the finite element. Recently, Loukidis et al. (2008) studied the bearing capacity of surface footings in sand subjected to eccentric and inclined loads using finite elements. They found that the inclination factor depends on the value of the friction angle, whereas the effective width does not. Most of the inclination factors i_γ and depth factors d_γ for cohesionless soil, available in the literature are given in Table 1.

Many researchers suggested examining the bearing capacity of shallow foundations under general loading, by expressing the applied loads in terms of combinations of vertical, horizontal, and moment loading (Bransby and Randolph 1998, 1999; Gourvenec 2008). The load combinations that caused failure were plotted as a failure envelope on an interaction diagram.

Research in the field of offshore foundations has more recently been carried out under drained load conditions. Using physical model testing, Gottardi and Butterfield (1993) performed laboratory tests on surface footings on very dense sand under general planar loads, using three dimensional small-scale models. They showed that the interaction diagram approach to bearing capacity estimation for surface footings enables an engineer to take into account the interaction between different loading components. Also, Gottardi and Butterfield (1995) proposed load-displacement data for surface footings on dense sand covering a sufficiently wide range of inclined, eccentric, eccentric-inclined and "non-radial" load-paths, (including "unloading" phases) for important conclusions to be drawn about. By using the three-degree-of-freedom loading Gottardi et al. (1999) presented

Table 1 Expressions of depth factor d_γ and inclination factor i_γ

Author	d_γ	i_γ
Meyerhof (1963)	$1 + 0.1\sqrt{N}\frac{D}{B}$	$\left(1 - \frac{z^\circ}{\phi}\right)^2 \alpha < \phi$
Hansen (1970)	1	$\left(1 - \frac{0.7H}{V+BLc_a \cot \phi}\right)^{\delta^2} c_a$: base adhesion $2 \leq \delta_2 \leq 5$
Vesic (1975)		$\left(1 - \frac{H}{V+BLc_a \cot \phi}\right)^{m+1} c_a$: base adhesion $m = \frac{2+B/L}{1+B/L}$
Lyamin et al. (2007)	$1 + (8.404 - 0.151\phi)\frac{D}{B}$	–
Loukidis et al. (2008)	–	$\left(1 - 0.94\frac{\tan z}{\tan \phi}\right)^{(1.5 \tan \phi + 0.4)^2}$

results of laboratory tests for circular footing under general planar loading on dense sand. They found that the shape of the yield surface is well described by a parabolic ellipsoid. Yun and Bransby (2003) presented results from a series of centrifuge model tests carried out to investigate the combined vertical, horizontal and moment loading response of skirted foundation on drained loose sand. They showed that the horizontal capacity of the skirted foundation was larger than that of raft foundation. There has been available little work studying the bearing capacity of embedded strip footings on cohesionless soil under combined loading.

The aim of this study is to directly investigate how variation in the embedment ratio (D/B) of a foundation affects its bearing capacity under inclined loadings in sand. To investigate this aspect of foundation behaviour, a series of finite difference analyses using the numerical code Fast Lagrangian Analysis of Continua (FLAC) (2005) were carried out for rigid foundations with different embedment ratio in sand. The friction angle and the inclination angle are varied carefully to cover most cases of practical interest. New information has been gained concerning the shape of the failure envelopes. The numerical results are compared with the available publications in the literature.

2 Numerical Modeling Procedure

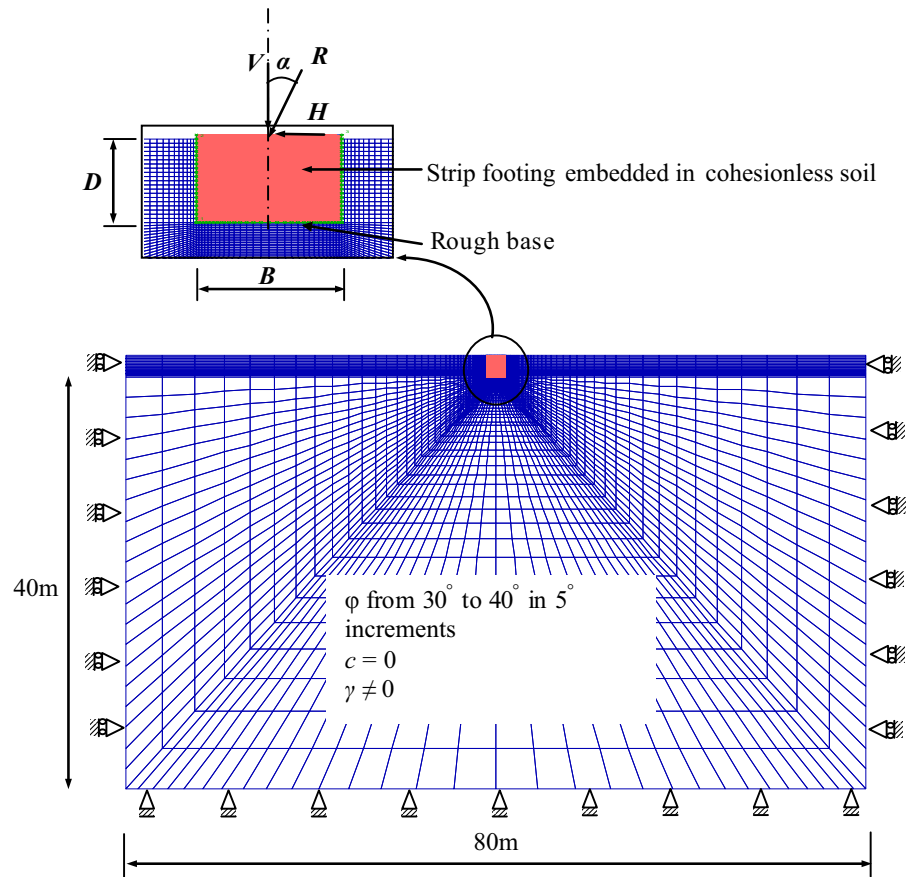
The problem studied considers strip footings embedded in cohesionless soil, under combined loading (vertical and horizontal loads), as shown in Fig. 1. In this paper, the finite-difference code FLAC (2005) was used to reach the bearing capacity for embedded rough strip footings. The finite-difference code Fast Lagrangian Analysis of Continua (FLAC) is a two-

dimensional program for geotechnical engineering; it simulates the behaviour of structures built of soil, rock or other materials that undergo plastic flow when their yield limits are reached.

In the current modeling study, the width B of the footing is 2 m and is embedded at a variable depth D. The embedment ratio D/B of 0 (surface), 0.25, 0.5, 0.75 and 1 were considered. Because of the absence of loading symmetry, the entire soil domain of dimensions (20B × 40B) is considered. Calculations for a larger mesh size indicated that extending the boundaries further away from the footing does not influence the computed limit load of the footing. The base of the model is constrained in all directions. The right and the left vertical sides are constrained in the horizontal direction only. The mesh adopted in the present study is shown in Fig. 1. The rigid footing is connected to the soil via interface elements defined by Coulomb shear-strength criterion. In the present study, the interface has a friction angle $\delta = \phi$ (perfectly rough soil-footing interface), a cohesion $c = 0$, a normal stiffness $K_n = 10^9$ Pa/m, and a shear stiffness $K_s = 10^9$ Pa/m.

The soil was considered to be a linearly elastic-perfectly plastic material, obeying Mohr–Coulomb criterion with the associative flow rule with a unit weight $\gamma = 20$ kN/m³. The soil elastic properties used are the shear modulus $G = 11.5$ MPa and the bulk modulus $K = 25$ MPa (equivalent to a Young’s modulus $E = 32$ MPa and a Poisson’s ratio $\nu = 0.3$). Mabrouki et al. (2010) indicated that the soil elastic parameters had a negligible effect on the value of the limit load of the strip footing; the only effect being that if the chosen values are high, the footing reaches the limit load at a smaller displacement. The friction angle ϕ was varied from 30° to 40° in 5° increments; for each value of the friction angle ϕ ,

Fig. 1 Finite-difference mesh used in the analyses for the case of $D/B = 0.5$



the dilation angle was set to $\phi = \psi$ (associative flow rule). The analyses with a non-associative flow rule were carried out using dilation angles ψ presented in Table 2. The footing elastic properties used are the Young's modulus $E = 25$ GPa and the Poisson's ratio $\nu = 0.4$. The values of the elastic parameters are large enough to ensure the rigid behavior of the foundation.

Both probe-type analyses and swipe-type analyses were carried out to identify the V–H failure envelope (where V and H are respectively the vertical and horizontal ultimate footing loads). In the first step of probe analyses, a vertical uniform stress (smaller than

q_u) is applied to the footing, then a damping of the system is introduced by running several cycles until a steady state of static equilibrium is developed in the soil. In second step a controlled horizontal velocity is applied to the nodes which discretize the footing. Displacement is increased until failure is reached. It is worthwhile noting that for displacement control, it is not possible to maintain a constant and predetermined value of the ratio H/V throughout the analysis.

Swipe tests, introduced by Tan (1990), are convenient, as a complete failure envelope in a two-dimensional loading plane can be determined in a single test. The swipe tests involve first bringing the foundation to vertical bearing failure, and subsequently applying horizontal velocity while not allowing the footing to move vertically.

The swipe analysis was originally introduced by Tan (1990) as an experimental technique and later used by some researchers (Bransby and Randolph 1998; Gourvenec and Randolph 2003). The benefit of this procedure of loading is that the failure envelope in

Table 2 Frictional angles and dilatancy angles used in finite difference analyses for non-associative flow rule

Friction angle ϕ (°)	Dilatancy angle ψ (°)	
	$\psi = 1/3 \phi$	$\psi = 2/3 \phi$
30°	10°	20°
35°	11.67°	23.33°
40°	13.33°	26.67°

the V–H space can be determined with one finite difference analysis runs. To define the failure envelope, two paths, path I and path II are required. The path I of swipe tests consists of two steps. In the first step the loading of the rigid footing is simulated by imposing equal vertical velocities at the nodes represented the footing. The progressive movement of the rigid footing induced by the vertical velocity applied at the footing nodes is accompanied by an increase of the pressure in the soil. Finally, the pressure under the footing stabilizes for a value that indicates the ultimate vertical load (V_{ult}). In the second step, horizontal velocity is applied until ultimate horizontal load is reached while not allowing the footing to move vertically. Furthermore, in the path II the horizontal velocity is applied to the footing without considering vertical loads, by using glued interfaces between the base for footing and soil. The two types of analyses are presented in Fig. 2.

3 Results and Discussions

3.1 Vertical Bearing Capacity of a Surface Footing

The numerical modeling procedure was first validated for the vertical bearing capacity problem. From Eq. (1), for a strip footing under vertical load on

cohesionless soil with no surcharge, the bearing capacity factor N_γ is:

$$N_\gamma = 2q_u/\gamma B \tag{3}$$

Figure 3 compares the bearing capacity factor N_γ for rough footings under vertical load with $\phi = 30^\circ, 35^\circ,$ and 40° . The present results of the bearing capacity factor N_γ , are obtained from calculations with the non-associative flow rule ($\phi = \psi$). We can observe that the results of the present study are in good agreement with the solutions reported by Terzaghi (1943). Also, the values of N_γ obtained from the present study are smaller than those obtained by Soubra (1999) and Bolton and Lau (1993). The solutions reported by Martin (2003) (using the method of characteristics) are significantly smaller than those determined by the present study. It is worthwhile noting that the refinement of mesh with a small vertical velocity produce a slightly better (lower values) results of N_γ . The present study produces good estimates of N_γ for surface strip footings.

3.2 Influence of Nonassociativity

It was confirmed by de Mabrouki et al. (2010), Erickson and Drescher (2002) and Yin et al. (2001) that the bearing capacity factors decreases with decreasing values of ψ . The effect of flow rule non-associativity ($\psi < \phi$) is illustrated in Fig. 4 in the

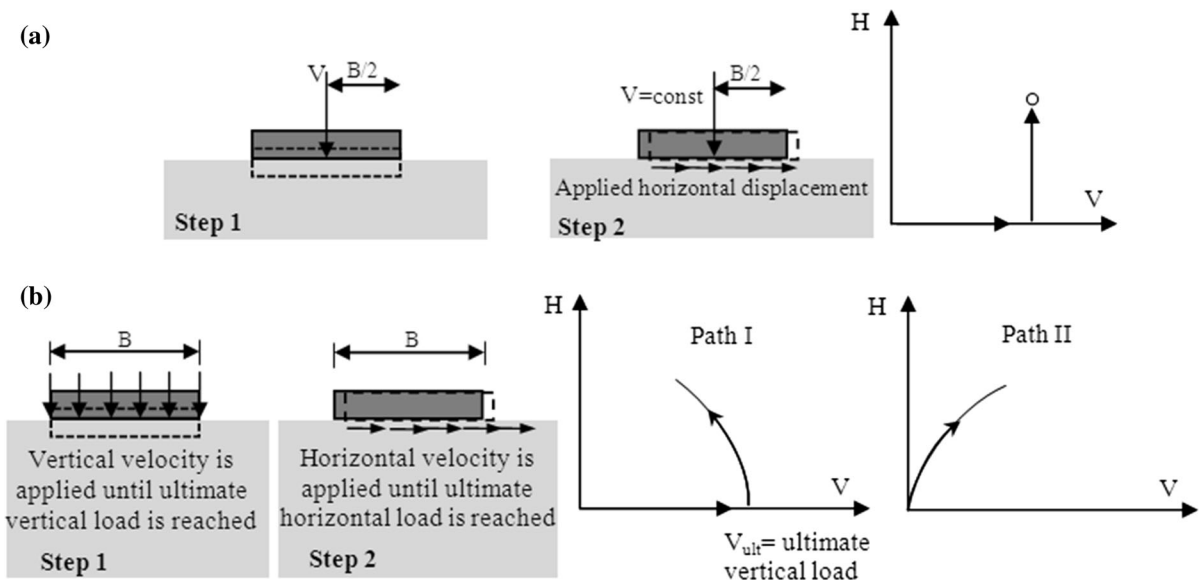


Fig. 2 Failure envelopes for V–H loading. a Probe analyses. b Swipe analyses

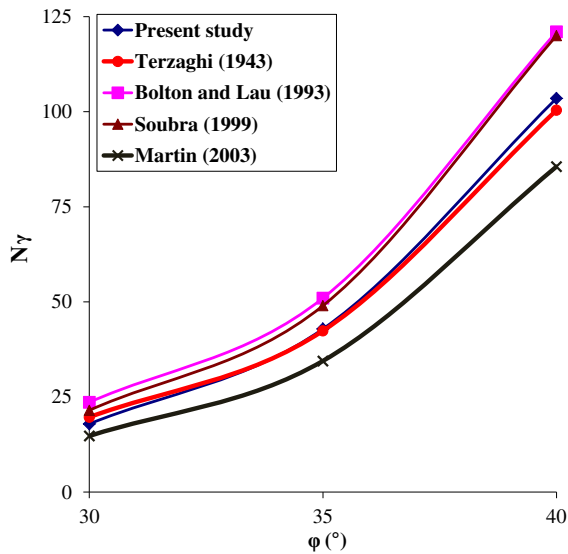


Fig. 3 Bearing capacity factor N_γ from finite difference analyses compared with other available theoretical predictions

form of load–displacement curves (i.e., the curves of the bearing capacity factor N_γ versus δ/B , where, δ is the vertical displacement). The friction angle ϕ equal to 35° , 40° with dilation angles $\psi = \phi/3$ and $\psi = \phi$ are used. It is seen that the N_γ values obtained from the analyses with the non-associative flow rule are lower than those with the associative flow rule, the difference increases with the increase of internal frictional angle ϕ of soil. It should be noted that for $\psi = \phi/3$, the curve of N_γ versus δ/B shows numerical oscillation, which can be attributed to the inherent numerical aspect of the FLAC code as explained by Yin et al. (2001). In this case the bearing capacity factor N_γ is calculated as a mean value within the range of the oscillations. The same tendencies are observed by Loukidis et al. (2008) and Mabrouki et al. (2010).

A second effect of the non-associative flow rule is shown by Fig. 5. The Figure presents the displacement vectors of the soil with friction angle $\phi = 35^\circ$ and for different values of ψ ($\psi = \phi$, $\psi = 2/3 \phi$, $\psi = 1/3 \phi$). It is noted that the value of the maximum magnitude of the displacement vectors (d_{\max}) varies with dilatancy angle ψ . With decreasing ψ , the displacements next to the footing edge decrease significantly. Figure 5a shows that for a large value of dilatancy angle ($\psi = \phi$), significant displacements are restricted to the exterior region close to the edge of the footing. As

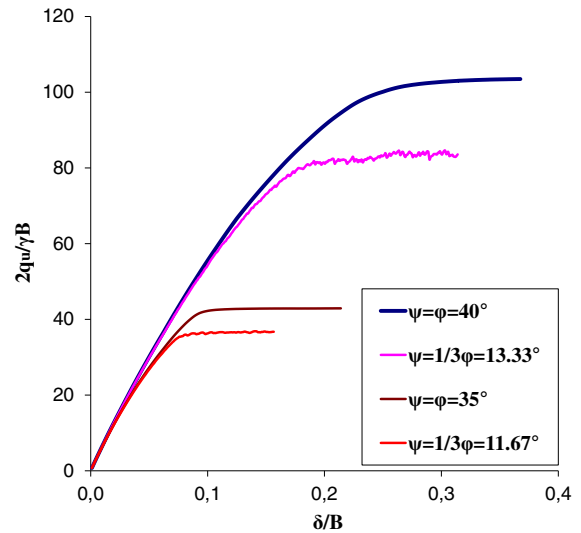


Fig. 4 Ratio $2q_u/\gamma B$ versus vertical displacement for rough footing, with friction angle, $\phi = 35^\circ$ and 40° and two values of dilation angle, $\psi = 1/3 \phi$ and $\psi = \phi$

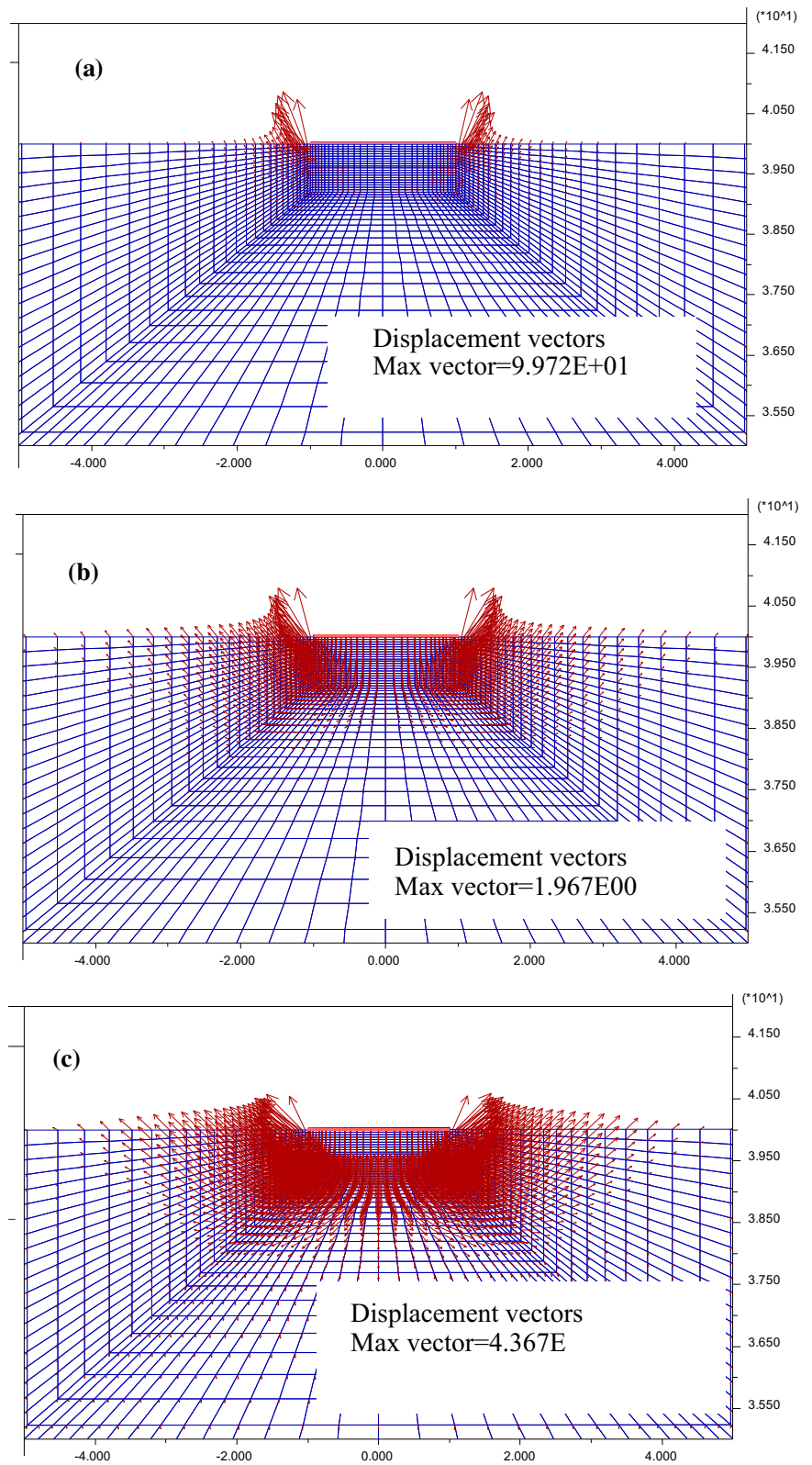
explained by Yin et al. (2001), the large value of displacement that occurred in the region of the footing edge may not be realistic but shall not affect the calculation of N_γ .

3.3 Effect of Load Inclination on the Bearing Capacity of a Surface Footing

3.3.1 Inclination Factor

The influence of load inclination on the bearing capacity of strip footings is estimated by inclination factor i_γ , defined as the ratio of the limit load for a strip footing under inclined loading $V_{ult,\alpha \neq 0}$ to that of the footing under centered vertical loads $V_{ult,\alpha=0}$ ($i_\gamma = V_{ult,\alpha}/V_{ult,\alpha=0}$). Figure 6 shows the inclination factors plotted against $\tan \alpha$ (H/V). It can be seen from this figure that i_γ decreases as the load inclination α increasing with a rate that is adequately captured by Hansen (1970). The numerical prediction obtained using the finite difference code FLAC is in good agreement with the factor of inclination proposed by Loukidis et al. (2008) based on the finite element. The results given by Vesić (1975) are reasonably close to the present results over a wide range of friction angles and load inclinations, though they are unconservative for high values of ϕ . For higher values of ϕ The

Fig. 5 Displacement vectors **a** $\psi = \varphi$; **b** $\psi = 2/3 \varphi$; **c** $\psi = 1/3 \varphi$



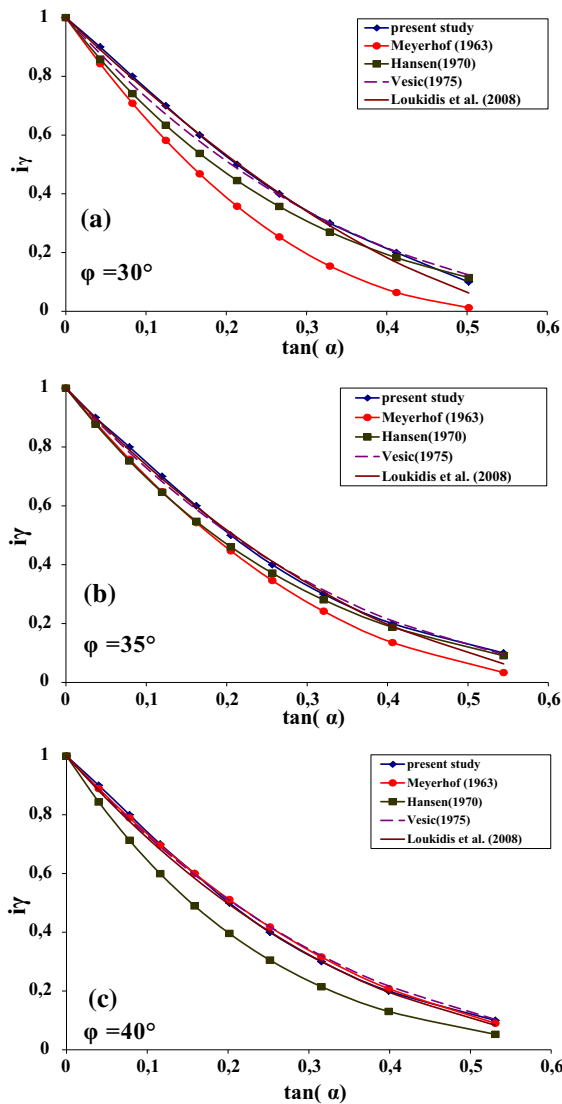


Fig. 6 Inclination factor as a function of the load inclination α **a** $\phi = 30^\circ$, **b** $\phi = 35^\circ$, and **c** $\phi = 40^\circ$

Hansen theory gives results which are always conservative. Moreover, the Meyerhof predictions are conservative for all values $\phi \leq 35^\circ$.

3.3.2 Failure Envelopes

The results from probe and swipe analyses of failure envelopes (called also yield surface) for different values of angle of friction ϕ are presented in Fig. 7. The paths generated from V–H (vertical load–horizontal load) swipe and probe analyses normalized with respect to the corresponding V_{ult} (Ultimate vertical

load). It is seen that the size and shape of the normalized V–H failure envelopes depend slightly on the value of frictional soil ϕ . It can also be observed from Fig. 7, that the results from the probe analyses are generally in good agreement with the swipe analyses.

Loukidis et al. (2008) assumed that there are no interface elements at the soil–footing contact plane, so any slippage between footing and soil occurs within the soil. Numerical analyses were performed to examine the shape of failure envelopes obtained with and without interface elements at the soil–footing contact. Figure 7 shows the good agreement between the results obtained with and without interface element. It is seen that the path II of swipe analysis, obtained by using an unlimited tensile resistance at the interface is similar to that obtained when no interface elements placed between the footing and the soil. Figure 8 shows the effect of non-associativity on the failure envelopes. It is clear that the analyses with a non-associative flow rule $\psi < \phi$, numerical oscillations in the path I are observed. Moreover, for the case of path I, there is poor agreement between the probe and swipe analyses.

Figure 9 presents the yield surface relating the applied vertical (V) and horizontal (H) loads from results of probe analyses normalized by division by V_{ult} . The Figure demonstrated that the load paths followed is remarkably close to a parabolic shape. A similar observation was presented by Gottardi et al. (1999) for circular footings on sand under general planar loading. The maximum value $H = 0.11V_{ult}$ and occur at $V/V_{ult} = 0.48$. It is worthwhile noting that the experimental values for H_{max} are of the order of

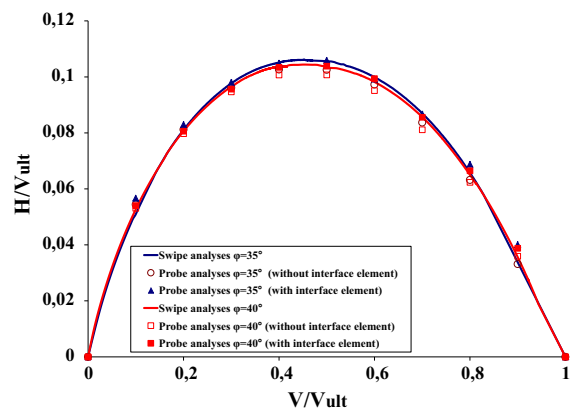


Fig. 7 Comparison between the present V–H failure envelope from probe and swipe analyses

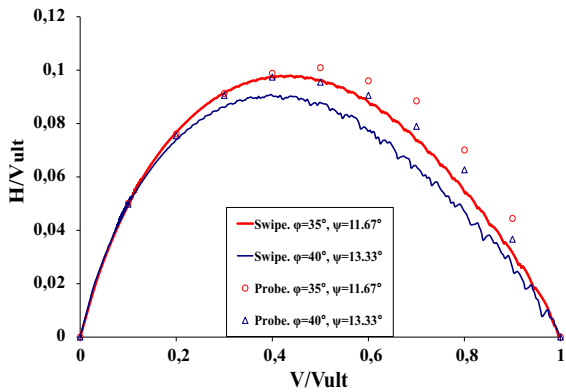


Fig. 8 Comparison of V–H failure envelopes for $\phi = 35^\circ, 40^\circ$ and $\psi = 1/3$

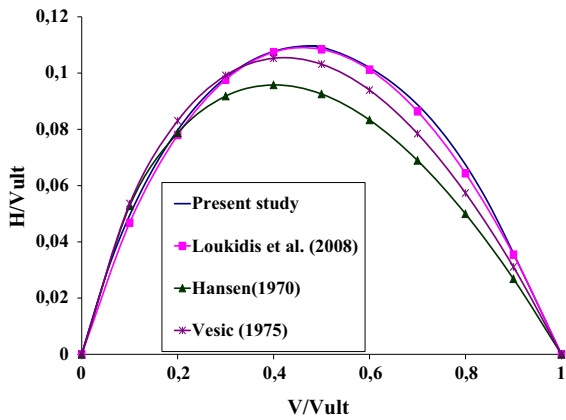


Fig. 9 Comparison of present V–H failure envelopes with those of Loukidis et al. (2008), Vesic (1975) and Hansen (1970) for $\phi = 30^\circ$ and $\psi = \phi$

$0.12V_{ult}$ (Gottardi and Butterfield 1993). The comparison of the present results with the existing solutions shows that the numerical simulations are very close to the results of Loukidis et al. (2008). However, the present solutions overestimate the results given by Hansen (1970) and Vesic (1975).

3.4 Effect of Load Inclination on the Bearing Capacity of Embedded Strip Footing

3.4.1 Depth Factor

The finite difference results are also used to derive depth factors d_γ . This is achieved by dividing the bearing capacities obtained for the footings at depth D by that obtained for the surface footing ($d_\gamma = V_{ult, D/B=}$

$V_{ult, D/B=0}$). Figure 10 shows the depth factor against D/B for the three values of friction angle ϕ considered. The relationship between d_γ and D/B is almost perfectly linear. Figure 9 proves that the degree of embedment affects significantly the bearing capacity of the foundation for a given value of frictional angle ϕ . More importantly it is seen that d_γ is greater than 1 and increases with increasing D/B for all values of friction angle ϕ . The values of d_γ proposed by Meyerhof (1963), Hansen (1970), Vesic (1975) and Lyamin et al. (2007) (for $\phi = 30^\circ$) are also presented. The depth factor d_γ was taken as 1 by both Vesic (1973) and Hansen (1970), as seen in Table 1. Conceptually, a value of $d_\gamma = 1$ means that the N_γ term refers only to the slip mechanism that forms below the base of the footing as explained by Lyamin et al. (2007). The values of depth factor found by finite difference analyses are larger than those proposed by Meyerhof (1963), Hansen (1970) and Vesic (1975) when the results of Lyamin et al. (2007) overestimate the influence of the embedment.

3.4.2 Inclination Factor

The effect of load inclination on bearing capacity of embedded strip footing in cohesionless soil is presented in Fig. 11. In this case, the load inclination factor i_γ , defined as the ratio of the limit load for embedded footings under inclined loading $V_{ult, \alpha \neq 0}$ to that of the embedded footing under centered vertical loads $i_\gamma = V_{ult(\alpha \neq 0, D/B \neq 0)} / V_{ult(\alpha = 0, D/B \neq 0)}$. Figure 11 shows the inclination factors obtained by swipe analyses for different values of ratios D/B (0 (surface),

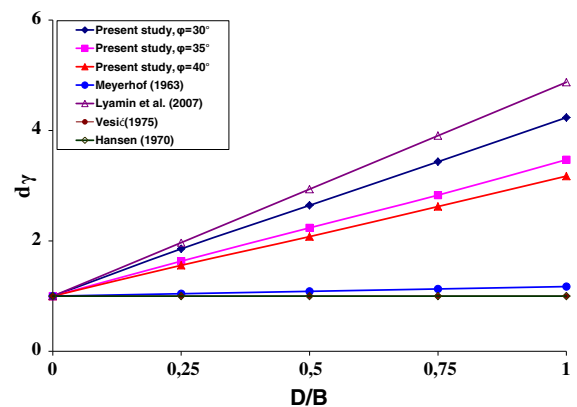


Fig. 10 Comparison of present d_γ values with those obtained from the expressions available in the literature

0.25, 0.5, 0.75 and 1). It is seen that for small values of load inclination the embedment depth does not significantly affect i_γ . However, for higher values of load inclination, the embedment depth produces inclination factors larger than those obtained for a surface footing; consequently, the footing embedment reduces the effect of load inclination.

3.4.3 Failure Envelopes

Figure 12 shows failure envelopes under combined vertical and horizontal load for each of the embedment ratios considered: $D/B = 0$ (surface), 0.25, 0.5, 0.75 and 1. As seen from Fig. 12a, the expansion of failure envelopes indicates the increased load-carrying capacity available with increased embedment ratio. The figure also clearly shows good agreement between the probe and swipe results, especially for $D/B \leq 0.75$. The normalized yield surface presented in Fig. 12b shows that the shape of the envelopes appears similar but is not unique. The size of the normalised envelope increases with increasing embedment ratio.

3.4.4 Failure Mechanisms

Figure 13 shows the contours of maximum shear strain for both surface and embedded footings under vertical or inclined loading. The elastoplastic finite difference analysis clearly show that different mechanisms depending on the loading conditions. It is noted that under displacement control, it is not possible to maintain a constant and predetermined value of the ratio H/V ($\tan \alpha$) throughout the analysis, for this a

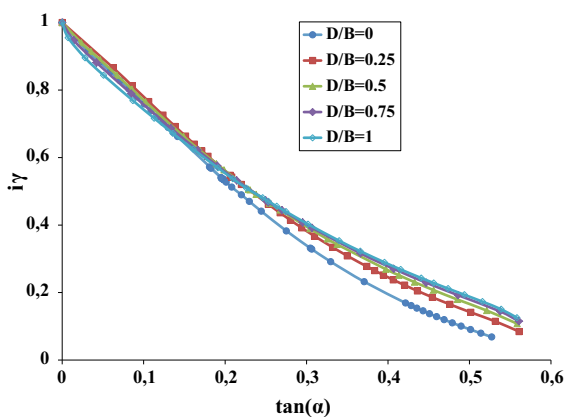


Fig. 11 Inclination factors of embedded footings for $\phi = 30^\circ$ and $\psi = \phi$

close values of α are presented. The size of the shear zone decreases with increasing of the load inclination. As seen from Fig. 13, for pure vertical loading ($\alpha = 0$), there is a triangular elastic wedge immediately underneath the footing and the shear zone is similar to the failure mechanism found by Prandtl (1920) and Terzaghi (1943). However, more $\alpha > 0$, the failure mechanism is asymmetrical and confined to one side of the footing for higher values of α . Also, it is observed that the value of the maximum magnitude of the displacement vectors varies with the depth of embedment: for larger depth the maximum displacement is higher.

4 Conclusions

The finite-difference code FLAC (2005) was used to study the bearing capacity for strip footing embedded in frictional soil under inclined loading. The soil used in the model was assumed to be a Mohr–Coulomb material with associative flow rule non-associative flow rules. Both probe-type and swipe-type analyses were carried out to identify failure envelopes under vertical and horizontal loading. The results are presented in terms of ultimate limit states. The numerical results are compared with ultimate loads predicted by the theories of Meyerhof, Hansen and Vesic and the available results published in the literature.

From the numerical study performed it is confirmed that the bearing capacity factor N_γ is very sensitive to the value of friction angle ϕ . The dilation angle has significant influences on the values of the bearing capacity factor N_γ . This effect is very important for higher values of the friction angle. The bearing capacity factors increases with the increasing of the dilation angle. The values of dilatation angle ψ affect the displacement vectors at failure of the strip footing, the displacements decrease with decreasing dilation angle.

The shape of the yield surface in V–H plane is well described by a parabolic form, as observed previously by Gottardi et al. (1999). The size and shape of the normalized V–H yield surface depends on the value of dilation angle. The normalized failure envelopes obtained with the associative flow rule, using the probe-type analyses are in very good agreement with those computed by swipe-type analyses; however, the

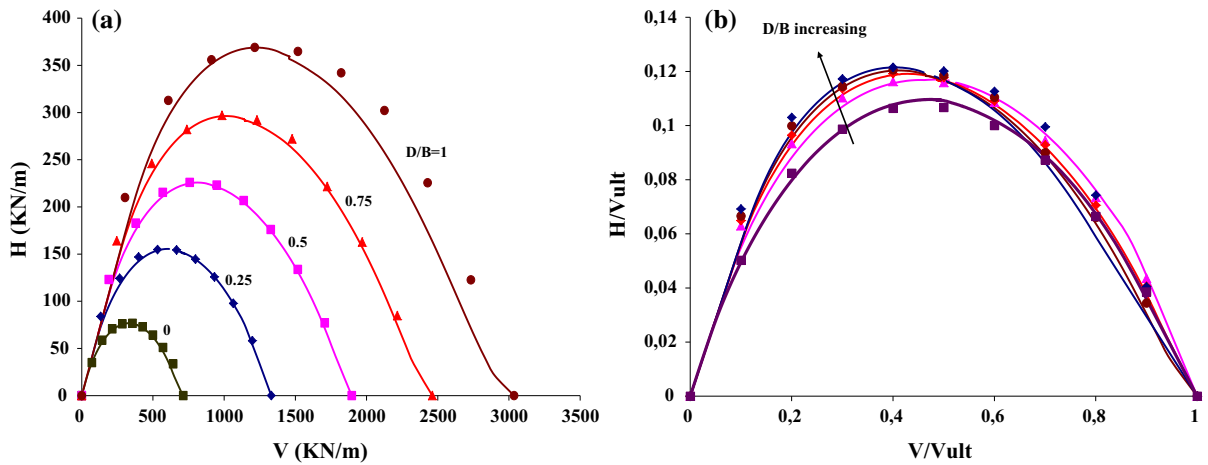


Fig. 12 Comparison between the present V–H failure envelopes from probe and swipe analyses for $D/B = 0, 0.25, 0.5, 0.75, 1$ for $\phi = 30^\circ$

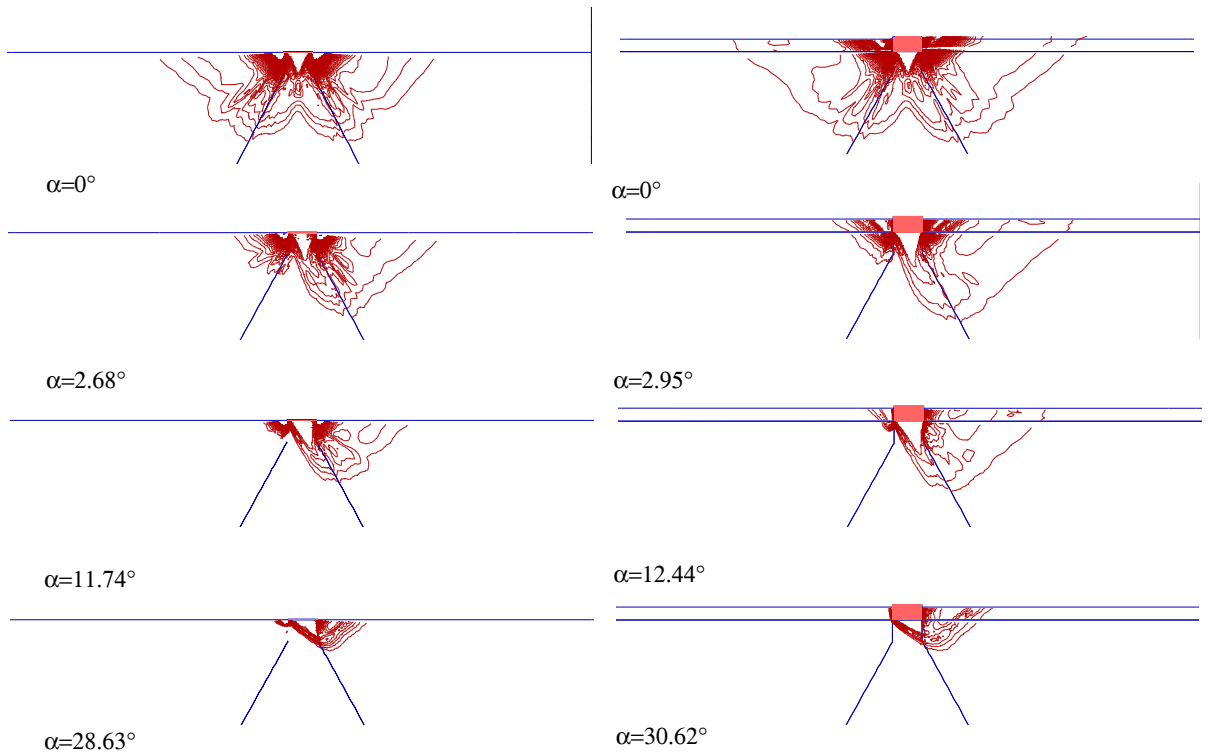


Fig. 13 Contours of maximum shear strain for different load inclinations for $\phi = 35^\circ$

discrepancy widens for non-associative flow rule. The finite difference analyses show that the size of failure envelopes for an embedded strip footing, under vertical and horizontal loading varies with the depth of embedment. The contours of the maximum shear

strain prove the existence of one sided failure mechanism for higher values of α , with the formation of an asymmetrical elastic wedge. The values of i_γ obtained from the present study for a surface footing are in good agreement with the solutions reported by Loukidis

et al. (2008). For higher values of load inclination the factor i_γ depends on the depth of embedment.

References

- Bolton MD, Lau CK (1993) Vertical bearing capacity factors for circular and strip footings on Mohr–Coulomb soil. *Can Geotech J* 30(6):1024–1033
- Bransby MF, Randolph MF (1998) Combined loading of skirted foundations. *Géotechnique* 48(5):637–655
- Bransby MF, Randolph MF (1999) The effect of embedment depth on the undrained response of skirted foundations to combined loading. *Soils Found* 39(4):19–33
- Chen WF (1975) *Limit analysis and soil plasticity*. Elsevier, Amsterdam
- Erickson HL, Drescher A (2002) Bearing capacity of circular footings. *J Geotech Geoenviron Eng ASCE* 128(1):38–43
- FLAC (2005) *Fast Lagrangian Analysis of Continua*, version 5.0. ITASCA Consulting Group, Inc., Minneapolis
- Frydman S, Burd HJ (1997) Numerical studies of bearing capacity factor N_γ . *J Geotechn Geoenviron Eng ASCE* 123(1):20–29
- Gottardi G, Butterfield R (1993) On the bearing capacity of surface footings on sand under general planar loads. *Soils Found* 33(3):68–79
- Gottardi G, Butterfield R (1995) The displacement of a model rigid surface footing on dense sand under general planar loading. *Soils Found* 35(3):71–82
- Gottardi G, Houlsby GT, Butterfield R (1999) Plastic response of circular footing on sand under general planar loading. *Géotechnique* 49(4):453–469
- Gourvenec S (2008) Effect of embedment on the undrained capacity of shallow foundations under general loading. *Géotechnique* 58(3):177–186
- Gourvenec S, Randolph MR (2003) Effect of strength nonhomogeneity on the shape and failure envelopes for combined loading of strip and circular foundations on clay. *Géotechnique* 53(6):575–586
- Hansen JB (1961) A general formula for bearing capacity. *Dan Geotech Inst Bull* 11:38–46
- Hansen JB (1970) A revised and extended formula for bearing capacity. *Dan Geotech Inst Bull* 28:5–11
- Hijaj M, Lyamin AV, Sloan SW (2005) Numerical limit analysis solutions for the bearing capacity factor N_γ . *Int J Solids Struct* 42(5):1681–1704
- Kumbhojkar AS (1993) Numerical evaluation of Terzaghi's N_γ . *J Geotech Eng* 119(3):598–607
- Loukidis D, Salgado R (2009) Bearing capacity of strip and circular footings in sand using finite elements. *Comput Geotech* 36(5):871–879
- Loukidis D, Chakraborty T, Salgado R (2008) Bearing capacity of strip footing on purely frictional soil under eccentric and inclined loads. *Can Geotech J* 45(6):768–787
- Lundgren H, Mortensen K (1953) Determination by the theory of plasticity of the bearing capacity of continuous footings on sand. In: *Proceedings of the third international conference on soil mechanics and foundation engineering*, Zürich, pp 409–412
- Lyamin A, Salgado R, Sloan SW, Prezzi M (2007) Two and three-dimensional bearing capacity of footings in sand. *Géotechnique* 57(8):647–662
- Mabrouki A, Benmeddour D, Frank R, Mellas M (2010) Numerical study of the bearing capacity for two interfering strip footings on sands. *Comput Geotech* 37(4):431–439
- Martin CM (2003) *User Guide for ABC—Analysis of Bearing Capacity*, Version 1.0. OUEL Report No. 2261/03. Department of Engineering Science, University of Oxford
- Meyerhof GG (1951) The ultimate bearing capacity of foundations. *Géotechnique* 2(4):301–332
- Meyerhof GG (1953) The bearing capacity of foundations under eccentric and inclined loads. In: *Proceedings of the 3rd international conference on soil mechanics and foundation engineering (ICSMFE)*, Zurich, vol I, pp 440–445
- Meyerhof GG (1963) Some recent research on the bearing capacity of foundations. *Can Geotechn J* 1(1):16–26
- Michalowski RL (1997) An estimate of the influence of soil weight on bearing capacity using limit analysis. *Soils Found* 37(4):57–64
- Michalowski RL (2005) Limit analysis in geotechnical engineering. In: *16th international conference on soil mechanics and geotechnical engineering (16th ICSMGE)*, TC-34 Rep, vol 5, pp 3679–3684
- Prandtl L (1920) *Über die Harte Plastischer Körper*. *Nachr. Ges. Wiss. Göttingen Math. Phys. Kl.* pp 74–85
- Soubra AH (1999) Upper-bound solutions for bearing capacity of foundations. *J Geotech Geoenviron Eng ASCE* 125(1):59–68
- Tan FS (1990) *Centrifuge and theoretical modelling of conical footings on sand*. PhD thesis, University of Cambridge
- Tani K, Craig WH (1995) Bearing Capacity of circular foundations on soft clay of strength increasing with depth. *Soils Found* 35(4):21–35
- Terzaghi K (1943) *Theoretical soil mechanics*. Wiley, New York
- Vesic AS (1973) Analysis of ultimate loads of shallow foundations. *J Soil Mech Found Div ASCE* 99(SM1):45–73
- Vesic AS (1975) Bearing capacity of shallow foundations. In: *Winterkorn HF, Fang H-Y (eds) Foundation engineering handbook*. Van Nostrand Reinhold, New York, pp 121–147
- Yin JH, Wang YJ, Selvadurai APS (2001) Influence of nonassociativity on the bearing capacity of a strip footing. *J Geotechn Geoenviron Eng ASCE* 127(11):985–989
- Yun GJ, Bransby MF (2003) Centrifuge modeling of the horizontal capacity of skirted foundations on drained loose sand. In: *Proceedings of the international conference on foundations*, Dundee, pp 1–10